



Roof weighting and support of a largely mined shallow coal seam

Ming Sun¹ · Ziqi Ye¹ · Xueliang Zhang² · Chen Guo¹ · Wenxiang Zheng¹ · Lei Qian¹

Received: 23 December 2021 / Accepted: 14 March 2022

Published online: 28 March 2022

© The Author(s) 2022

Abstract

To study roof weighting and the support of a largely mined shallow coal seam, the hydraulic support resistances in both small and large periodic weightings were derived by different theoretical formulae. Support working resistances of the 12,401 mining face in small and large periodic weighting were 10,442 and 17,064 kN, which represented a loading-increase coefficient of up to 1.64. Mining cracks were formed up to land surface and were visible to the naked eye, and numerical simulation of roof stratum structure by 3DEC has been proven to be realistic. A 1.2-MPa supporting intensity represented a critical threshold for effectively reducing horizontal displacement and inhibiting rib spalling using FLAC^{3D}. Hydraulic fracturing and micro-seismic monitoring were used to ensure the safety of the 12,401 mining face. These findings can explain the mechanism of mining a shallow coal seam for effective prevention and controlled design. The results show high accuracy and are consistent with reality.

Keywords Mining · Roof weighting · Support · Shallow coal seams · Big periodic weighting · Small periodic weighting

1 Introduction

It is well known that largely mining shallow coal seams are being widely used in China's main northwest coal-production area [1]. It has many advantages such as productivity, lower amounts of discharged gangue, and less coal dust: problems include severe rib spalling, frequent support crushing, and roof water disasters [2]. More research has been developed in recent years: Yang [3] revealed the specific mechanism of main roof weighting with a large mining height, Huang et al. [4] investigated the cantilever fracture pattern of the equivalent immediate roof. He et al. [5] conducted physical simulation experiments of roof breaking angles from 56.2 to 69.3°, Huang et al. [6] proposed a method of determining the reasonable support load and rated working resistance. He et al. [5] established mechanical models for key strata and equivalent immediate roof of large-mining-height working faces in a shallow coal seam.

Yin [7] established a cutting block model for hydraulic supports. Wen et al. [8] proposed a method for determining support working loads under given deformation and limited deformation. Liu et al. [9] estimated the effects of mining face length and the underground pressure distribution when mining over a large height. Wang and Pang [10] discussed the mining or caving method for use in a thick coal seam, Wang et al. [11] evaluated coal rib stability effects over large mining heights, Xu et al. [12] explored the supporting stress fields with large mining height using an elastic beam model. Fan et al. [13] established a mining intensity evaluation model for coal seams with a large mining height. Wang et al. [14] investigated the relationship of hydraulic supports to the coal wall in coal seams with a large mining height, Zhao et al. [15] simulated the undermined ground pressure distribution on geographic information system, Kong et al. [16] determined the specific support capacity needed for the stability control of a

✉ Ming Sun, sunming831130@126.com | ¹Inner Mongolia University of Science and Technology, Baotou 014010, Inner Mongolia, China. ²Beijing Tianma Intelligent Control Technology Co., Ltd, Beijing 101399, China.



coal face, Huang and Tang [17] assessed the mining roof structural changes in a shallow coal seam, Zhang et al. [18] studied the roof leakage mechanism of fully mechanized faces with a large mining height. Huang and Zhou [19] explored the roof weighting behavior and patterns of largely mined-out shallow coal seams, Wang et al. [20] discussed the effects of broken key strata. Yang et al. [21] investigated the strata failure process and the required support resistance, Guo et al. [22] discussed the given mechanism of overburden strata deformation with a large mining height around geological structures. Wang et al. [23] elucidated mechanisms of rib spalling through different types of faults, Xie et al. [24] debated different characteristics of strata movement and support systems. Yang and Kong [25] studied the reinforcement mechanism of rib spalling, Chang et al. [26] discussed the different rib spalling mechanisms of fully mechanized top caving seams with and large mining height, Yin et al. [27] studied the different criteria and safety evaluation of rib spalling in shallow coal seams. RayChowdhury et al. [28] got visible light communication and long rang wireless technology for transmitting underground information to the above-ground control room.

Roof stratum control in shallow coal seams has been effective, but the relationship between roof weighting and support strength remains to be found in specific geological conditions. In the present work, hydraulic support working resistances in small and large periodic weightings were determined. Numerical simulations in 3DEC and FLAC^{3D} were used to reveal specific mechanism of roof weighting and support intensity in mining shallow coal seams. These findings explain the mechanisms prevailing when mining shallow coal seams for effective accident prevention and controlled design.

2 Roof weighting and support resistance in small or large periodic weightings

2.1 Roof weighting and support resistance under small periodic weighting

The immediate roof stratum of a shallow coal seam is regarded as the likely rigid body or the given load stratum over the hydraulic support, and the main roof stratum is considered to be the given deformation stratum above the immediate roof and hydraulic support [29]. The morphological structures of a composite cantilever beam and a hinged rock beam in small periodic weightings are shown in Fig. 1. In small periodic weightings, hydraulic supports are never up to the maximum pressure, so the safety valve is less likely to open and roof subsidence remains under control [30]. The maximum support pressure is bearing the

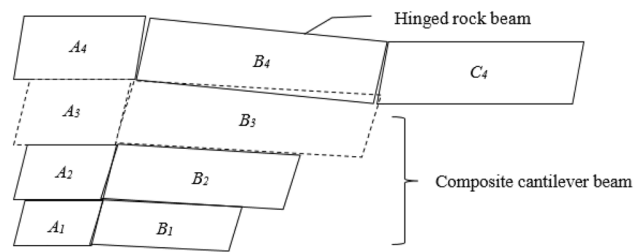


Fig. 1 Morphological structure of a composite cantilever beam and hinged rock beam in small periodic weighting

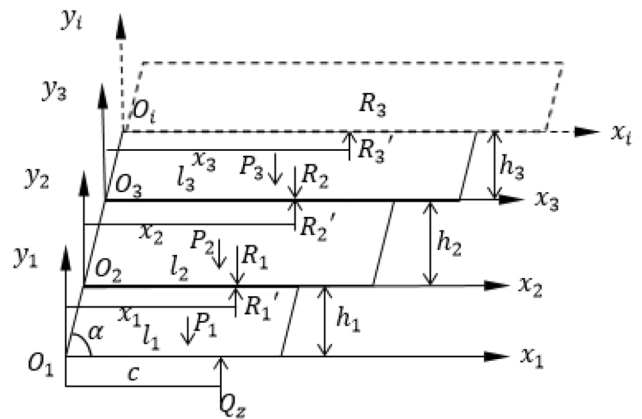


Fig. 2 Mechanical analysis of a composite cantilever beam in small periodic weighting

whole load of immediate roof stratum and the part-load of the main roof stratum. In Fig. 1, the immediate roof stratum is seen as the composite cantilever beam including blocks $A_1, B_1, A_2, B_2, A_3,$ and B_3 . Blocks $A_1, A_2,$ and A_3 are firstly formed above the coal seam. Blocks $B_1, B_2,$ and B_3 are then formed above the hydraulic support. The main roof stratum is usually regarded as a hinged rock beam formed from blocks $A_4, B_4,$ and C_4 , which are above A_3, B_3 and mined gob. Block A_4 is first formed above A_3 , block B_4 is then formed above B_3 , and block C_4 is finally formed above the mined gob.

Mechanical analysis of composite cantilever beams in small periodic weighting is illustrated in Fig. 2. Points $O_1, O_2,$ and O_3 are the fracture locations of A_1 and B_1, A_2 and B_2, A_3 and B_3 . $x_1O_1y_1, x_2O_2y_2,$ and $x_3O_3y_3$ are the rectangular coordinate systems of $B_1, B_2,$ and B_3 . Q_z is the hydraulic support pressure, c denotes the distance between a hydraulic support and fracture location O_1 , α is the roof fracture angle, l_1 is the length of B_1 , h_1 represents the depth of B_1 , p_1 is the weight of B_1 , R_1 and R'_1 denote the added loads from B_2 , l_2 is the length of B_2 , h_2 refers to the depth of B_2 , p_2 is the weight of B_2 , R_2 and R'_2 are the added

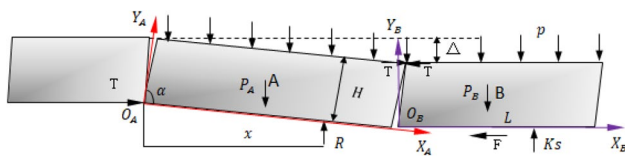


Fig. 3 Mechanical analysis of a hinged rock beam in small periodic weighting

loads from B_3 , and $R_j = R'_j (j = 1, 2, \dots, n)$ is the internal force on the immediate roof stratum.

The immediate roof stratum reaches a mechanical equilibrium as given by formulae (1–6).

$$\sum M_{oi} = 0 (i = 0, 1, 2, \dots, n) \tag{1}$$

$$Q_{z1}c - R_1x_1 - P_1 \left(\frac{l_1}{2} + \frac{h_1}{2} \cot \alpha \right) = 0 \tag{2}$$

$$R'_1(x_1 - h_1 \cot \alpha) - R_2x_2 - P_2 \left(\frac{l_2}{2} + \frac{h_2}{2} \cot \alpha \right) = 0 \tag{3}$$

$$R'_2(x_2 - h_2 \cot \alpha) - R_3x_3 - P_3 \left(\frac{l_3}{2} + \frac{h_3}{2} \cot \alpha \right) = 0 \tag{4}$$

$$R'_{n-1}(x_{n-1} - h_{n-1} \cot \alpha) - R \cdot x - P_n \left(\frac{l_n}{2} + \frac{h_n}{2} \cot \alpha \right) = 0 \tag{5}$$

$$Q_{z1} \cdot c = \sum_{i=1}^n P_i \left(\frac{l_i}{2} + \frac{h_i}{2} \cot \alpha \right) + \sum_{i=1}^{n-1} R_i h_i \cot \alpha + Rx \tag{6}$$

Q_{z1} is the hydraulic support pressure, P_j is the weight of the immediate roof stratum, h_j represents the thickness of the immediate roof stratum, l_j denotes the immediate roof stratum length, α is the roof stratum fracture angle, C represents the distance between the support force and coal wall, and R is the added load from the main roof stratum. The roof stratum interactive force can be omitted, so the immediate roof and main roof can be generalized as an integrated whole; formula (6) is simplified to the form given in (7). Mechanical analysis of a hinged rock beam under small periodic weighting is shown in Fig. 3, and it can be regarded as a hinged structure.

$$Q_{z1} = \frac{\sum_{i=1}^n P_i \left(\frac{l_i}{2} + \frac{h_i}{2} \cot \alpha \right) + Rx}{c} \tag{7}$$

The relationship between blocks A and B can be generalized by formulae (8–10).

$$\begin{cases} Rx - (P_A + p)L \left(\frac{L}{2} + \frac{H}{2} \cot \alpha \right) + T(H - \Delta) = 0 \\ KsL - (P_B + pL) + Tf = 0 \end{cases} \tag{8}$$

$$T = \frac{p + L(P - Ks)}{f} \tag{9}$$

$$Rx = \frac{pLf(L + H \cot \alpha) - (p + LP - LKs)(H - \Delta)}{f} \tag{10}$$

Key blocks A and B are the same length and depth in small and large periodic weightings, so $P_A = P_B = P$. Taking formulae (9) into (10), the hydraulic support working resistance under small periodic weighting over a large mining height is given by formula (11).

$$Q_{z1} = \frac{f \sum_{j=1}^{i+1} P_j (l_j + h_j \cot \alpha) + pLf(L + H \cot \alpha) - 2(P + pL - KsL)(H - \Delta)}{2cf} \tag{11}$$

where L is the periodic weighting interval, H is the key block depth, P represents the key block weight, p denotes the upper uniform load, f is the block friction coefficient, K represents the gob gangue stiffness, s is the gob gangue compression, $s = (k_1 - k_2) \sum_{j=1}^i h_j$, k_1 is a stratum expansion coefficient, k_2 is a residual expansion coefficient, Δ is the compression of block A, $\Delta = m\eta + (1 - k_1) \sum_{j=1}^i h_j$, η is the coal recovery ratio, and m is the large mining height.

2.2 Roof weighting and support resistance under large periodic weighting

Chinese mining of shallow coal seams usually advances by 15 to 20 m a day, so the collapsed roof stratum cannot fully backfill gob which is then poorly compacted after being periodically broken. In big periodic weightings, hydraulic supports are usually up to the maximum pressure, so the safety valve is often likely to open and roof subsidence is out of control [30]. Key stratum caving spans are much longer than periodic weighting intervals, so the broken roof stratum conforms to an elastic long beam model ([31] in Fig. 4 (a) showing the mechanical analysis, and (b) the compressed analysis).

S is the compression degree of the elastic long beam and breaking roof stratum, which can be described by parabolic functions from O to L . K_j is compression stiffness of key block A, $P_{(x)}$ is the force acting between the beam and surrounding rock stratum (formula 12):

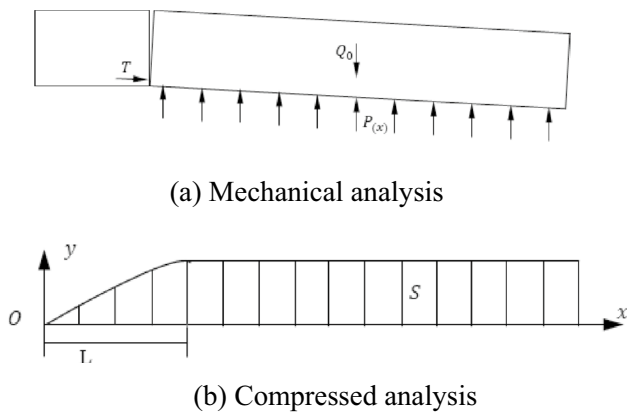


Fig. 4 Mechanical and compressed analyses of an elastic beam under large periodic weighting

$$P_{(x)} = K_{(x)}y_{(x)} = \begin{cases} K_j s \sqrt{\frac{x}{L}} & ; 0 \leq x \leq L \\ KS & ; L < x \leq L_0 \end{cases} \quad (12)$$

L_0 is the span of the beam, x is the distance from the coordinate origin to the point of contact between the long beam and caving gangue, K_j refers to the bracing stiffness of the roof, support and floor. The main roof stratum is synchronously broken by the elastic long beam, whose lower strata are considered as a composite cantilever beam. The upper strata of the long beam are considered as an articulated set of rock blocks, so a long beam model can be considered as a cantilever beam-articulated block system (formula 13).

$$Q_{z2} \cdot cf = \sum_{j=1}^n P_j \left(\frac{l_j}{2} + \frac{h_j}{2} \cot \alpha \right) + R_{\text{longbeam}} x_{\text{longbeam}} \quad (13)$$

R_{longbeam} is the internal force between the long beam and the lower block (formula 14), x_{longbeam} denotes the virtual distance from the point of contact to that where the force acts between the long beam and the rock stratum.

$$R_{\text{longbeam}} x_{\text{longbeam}} = \frac{2}{3} K_j s L_0 \quad (14)$$

Taking formula (14) into (13), the hydraulic support working resistance under large periodic weighting when mining a shallow coal seam is given by formula (15).

$$Q_{z2} = \frac{9 \sum_{j=1}^n P_j (l_j + h_j \cot \alpha) \left[1 + K_z / \left(\sum_{j=1}^{i+1} h_{iE_j} + h_{fE_f} \right) \right] + 12SL_0 K_z}{18cf \left[1 + K_z / \left(\sum_{j=1}^{i+1} h_{iE_j} + h_{fE_f} \right) \right]} \quad (15)$$

P_j is the immediate roof block weight, h_j is the immediate roof block depth, l_j is the immediate roof block length, α is the roof rock fracture angle, K_z represents the compression

stiffness, h_i is the roof stratum depth below the key strata, E_i refers to the roof stratum elastic modulus below the key strata, h_f is the immediate floor depth, E_f is the immediate floor elastic modulus, S is the caving rock compression caused by the long beam, L_0 is the long beam caving length, and C denotes the distance between the line of action of the resultant force and the coal wall.

Because $\frac{\lim K_z}{\left(\sum_{j=1}^{i+1} h_{iE_j} + h_{fE_f} \right)} = 0$ and $1 + \frac{K_z}{\left(\sum_{j=1}^{i+1} h_{iE_j} + h_{fE_f} \right)} = 1$, the hydraulic support working resistances under large periodic weighting over a large mining height are given by formula (16).

$$Q_{z2} = \frac{9 \sum_{j=1}^n P_j (l_j + h_j \cot \alpha) + 12SL_0 K_z}{18cf} \quad (16)$$

3 Numerical simulations of the roof structure by 3DEC and support load by FLAC^{3D}

3.1 Numerical simulation of roof stratum structure by 3DEC

3DEC software is used to simulate large differential displacements, which can allow multiple contact modes, providing multiple material models [32]. Numerical simulation of this roof stratum structure by 3DEC covered a 300-m long, 1-m wide, 237-m high model. The mining height of the 12,401 seam is 8.8 m, the roof stratum is 215 m deep, and the Mohr-Coulomb yield criterion is used. The related rock mass physico-mechanical parameters are listed in Table 1, and rock mass joint fissure parameters are displayed in Table 2.

When the stimulation reached 50,000 feet (15.24 km), the mining roof stratum can be broken and collapsed by longwall caving method. Considering the boundary effect, coal mining begins from 50 m to the left until 50 m to the right, giving an excavation length of 200 m. The roof stratum structure simulation is illustrated in Fig. 5 showing 113,637 steps: (a) is the initial model diagram; (b) is the roof failure distribution, and (c) is the roof displacement distribution. Discontinuous surface cracking of the 12,401 ground subsidence basin is shown in Fig. 6. The height of the water-induced fracture zone exceeds 200 m, so mining cracks reach the land surface, and are visible to the naked eye. This arises because the arc-shaped separation space is not even, one big periodic weighting of the large mining height usually appears after two or three small periodic weightings: the main and inferior key strata are broken and collapsed by the longwall caving method.

Table 1 Rock mass physico-mechanical parameters

Parameter Lithology and depth	Density d / kg/m^{-3}	Elastic modu- lus K /GPa	Shear modulus G /GPa	Cohesion c /MPa	Internal friction angle φ (°)	Tensile strength σ_T / MPa
Cobbles 50 m	2500	10.1	7.0	1.72	39	1.70
Coarse-grained sandstone 6 m	2500	4.0	2.6	0.73	35	0.37
Mudstone 12 m	2000	4.4	2.9	0.79	34	0.41
Coarse-grained sandstone 6 m	2500	4.0	2.6	0.73	35	0.37
Mudstone 32 m	2000	4.4	2.9	0.79	34	0.41
Coarse-grained sandstone 2 m	2500	4.0	2.6	0.73	35	0.37
Sandy mudstone 21 m	2000	4.4	2.9	0.79	34	0.41
Coarse-grained sandstone 4 m	2500	4.0	2.6	0.73	35	0.37
Sandy mudstone 18 m	2000	4.4	2.9	0.79	34	0.41
Coarse-grained sandstone 3 m	2500	4.0	2.6	0.73	35	0.37
Sandy mudstone 6 m	2000	4.2	2.5	1.03	37	0.54
Coarse-grained sandstone 5 m	2500	5.7	3.9	1.44	38	0.75
Mudstone 11 m	2000	6.9	4.8	1.30	38	0.67
Siltstone 3 m	2500	6.6	4.8	1.49	38	0.76
Mudstone 9 m	2000	6.9	4.8	1.30	38	0.67
Coarse-grained sandstone 4 m	2500	6.6	4.8	1.49	38	0.76
Siltstone 16 m	2000	6.9	4.8	1.30	38	0.67
Fine-grained sandstone 6 m	2500	6.6	4.8	1.49	38	0.76
Mudstone 0.5 m	2000	6.9	4.8	1.30	38	0.67
12 coal seam 8.8 m	1380	13.9	13.0	5.7	22	0.93
Mudstone 1.22 m	2000	6.9	4.8	1.30	38	0.67
Sandy mudstone 5 m	2000	6.9	4.8	1.30	38	0.67

So numerical simulation of this roof stratum structure by 3DEC is shown to conform to the reality in this mine.

3.2 Numerical simulation of graded support load by FLAC^{3D}

FLAC^{3D} is an explicit finite-difference formulation used to imitate complex behaviors, but some problems include several stages, large displacements, and nonlinear material behaviors [33]. According to the 12,401 seam mining information and exploration borehole histogram, support pressures upon coal failure, as modeled by FLAC^{3D} reached 0.5 MPa under similar operational conditions, when using similar working procedures. This operation was covered a 200-m long, 1-m wide 237-m high model (Tables 1 and 2), whose upper strata were 1-m long, 1-m wide in Figs. 7 and 8. Figure 7a shows the initial stress equilibrium, Fig. 7b illustrates the vertical stress distribution at 200 m, Fig. 8a shows the horizontal displacement at an 8.8-m mining height, Fig. 8b demonstrates the vertical displacement at an 8.8-m mining height, the 0.1-0.9-1.3 MPa pressure on the uppermost five rock blocks was used instead of the support afforded by each hydraulic support to the roof;

support pressures P at coal failure are shown in Fig. 9, (a) $P=0.8$ MPa, (b) $P=1.0$ MPa, (c) $P=1.2$ MPa, (d) $P=1.4$ MPa.

When P was 0.8 MPa, the immediate roof stratum was mainly broken in the front of the hydraulic support, and partial rib spalling was less likely to happen. The shear failure range of the coal seam was decreased, tensile failure occurred within 1 m in front of the coal wall, but the worst extent of failure remained in the central coal wall.

When P was 1 MPa, the shear failure range and roof subsidence velocity in the immediate roof stratum decreased. Tensile failure mainly occurred within 1 m in front of the coal wall, but the greatest extent of failure remained in the middle of the coal seam.

Figure 10 shows contours of szz at 30 m when P is 1.2 MPa; (a) shows contours of szz at 30 m and (b) shows contours of szz at 130 m. The shear failure range and roof subsidence velocity in the immediate roof stratum had been effectively controlled, but the immediate roof stratum was mainly broken next to the hydraulic support. The worst failure still occurred in the middle of the coal wall, penetrating to a depth of about 1.0 m.

When P was 1.4 MPa, the non-shear failure range of the immediate roof stratum was increasing, and the immediate roof stratum was mainly broken above the rear of the

Table 2 Rock mass joint fissure parameters

Parameter Lithology and depth	Normal stiffness <i>n</i> /GPa	Tangential stiffness <i>Ks</i> /GPa	Cohesion <i>c</i> /MPa	Internal friction angle ϕ (°)	Tensile strength σ_T / MPa
Cobbles 50 m	2	2	0.172	39	0.170
Coarse-grained sandstone 6 m	0.2	0.2	0.073	35	0.037
Mudstone 12 m	0.1	0.1	0.079	34	0.041
Coarse-grained sandstone 6 m	0.2	0.2	0.073	35	0.037
Mudstone 32 m	0.1	0.1	0.079	34	0.041
Coarse-grained sandstone 2 m	0.2	0.2	0.073	35	0.037
Sandy mudstone 21 m	0.1	0.1	0.079	34	0.041
Coarse-grained sandstone 4 m	0.2	0.2	0.073	35	0.037
Sandy mudstone 18 m	0.1	0.1	0.079	34	0.041
Coarse-grained sandstone 3 m	0.2	0.2	0.073	35	0.037
Sandy mudstone 6 m	0.1	0.1	0.103	37	0.054
Coarse-grained sandstone 5 m	0.2	0.2	0.144	38	0.075
Mudstone 11 m	0.1	0.1	0.130	38	0.067
Siltstone 3 m	0.2	0.2	0.149	38	0.076
Mudstone 9 m	0.1	0.1	0.130	38	0.067
Coarse-grained sandstone 4 m	0.2	0.2	0.149	38	0.076
Siltstone 16 m	0.1	0.1	0.130	38	0.067
Fine-grained sandstone 6 m	0.2	0.2	0.149	38	0.076
Mudstone 0.5 m	0.1	0.1	0.130	38	0.067
12 coal seam 8.8 m	0.1	0.1	0.57	22	0.093
Mudstone 1.22 m	1	1	0.130	38	0.067
Sandy mudstone 5 m	1	1	0.130	38	0.067

hydraulic powered support. The worst extent of failure remained in middle of the coal wall, penetrating to a depth of about 0.5 m.

Provided the supporting intensity is less than 1.2 MPa (Table 3), horizontal displacement in coal wall gradually decreased with increasing support pressure. When *P* was greater than 1.2 MPa, the horizontal displacement of the coal wall would be stable with increasing support pressure, so 1.2 MPa could be seen as the critical threshold at which engineers could effectively reduce horizontal displacement and inhibit rib spalling. Numerical simulation of graded support load by FLAC^{3D} is well able to identify the optimum support pressures upon coal failure.

4 Engineering calculation and verification

4.1 Engineering calculation

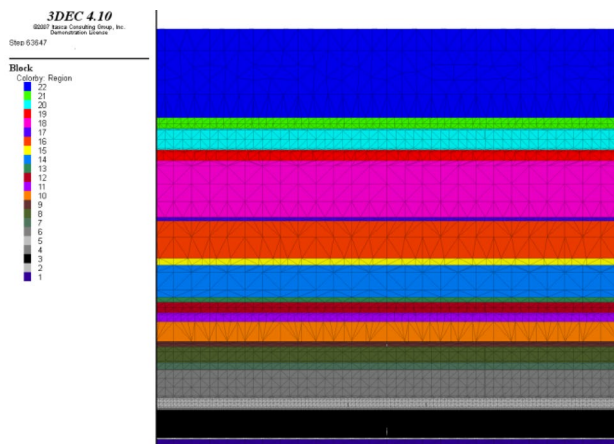
Shangwan Colliery is located in Ordos Ejinholo, Inner Mongolia; the overlying stratum of the 12,401 mining face has a thickness ranging from 124 to 244 m, the thickness of its loose layer ranges from 0 to 27 m k, and

the dip angle ranges from 1 to 5°. The designed mining height of the 12,401 face is 8.8 m, its coal mining length is 299.2 m, the advanced mining length reaches 5254.8 m, and the predicted mining production is up to the historical record of 17.58 Mt.

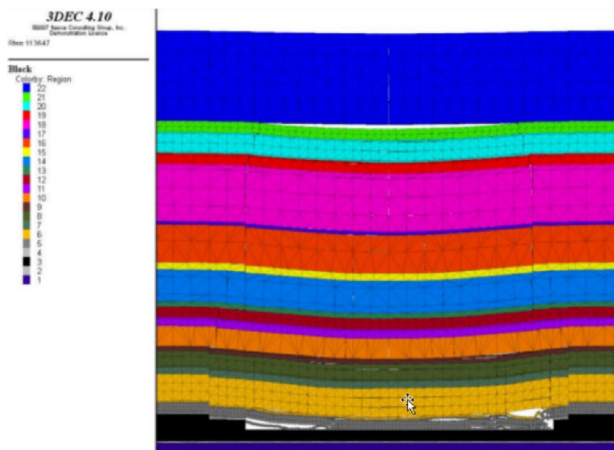
According to site investigation, *f* is 0.5, $\sum P_j$ is 2000 kN, $\sum l_j$ is 6 m, $\sum h_j$ is 3 m, α is 60°, *p* is 20 kN/m³, *L* is 10 m, *H* is 5 m, *P* is 200 kN, *K* is 40 kN/m³, *s* is 0.3 m, Δ is 8 m, and *c* is 1 m. The 12,401 hydraulic support working resistances under small periodic weightings over a large mining height are given by formula (11).

$$\begin{aligned}
 Q_{z1} &= \frac{f \sum_{j=1}^{i+1} P_j (l_j + h_j \cot \alpha) + pLf(L + H \cot \alpha)}{2cf} \\
 &- \frac{2(P + pL - KsL)(H - \cot \alpha)}{2cf} \\
 &= \frac{9278\text{KN} + 1030\text{KN} + 1680\text{KN}}{1\text{m}} \\
 &= 10442\text{KN}
 \end{aligned}$$

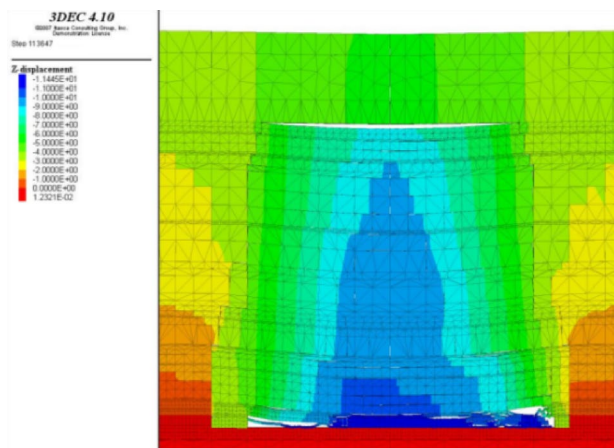
According to site investigation, *c* is 1 m, *f* is 0.5, $\sum P_j$ is 2000 kN, $\sum l_j$ is 6 m, $\sum h_j$ is 3 m, α is 60°, *S* is 3 m, *L*₀ is 10 m,



(a) Initial model diagram



(b) Roof failure distribution



(c) Roof displacement distribution

Fig. 5 Roof stratum structure simulation



Fig. 6 Discontinuous surface cracking of the 12,401 ground subsidence basin

and K_z is 40 kN/m^3 . The 12401 hydraulic support working resistances under large periodic weighting over a large mining height are given by formula (16).

$$\begin{aligned}
 Q_{z2} &= \frac{9 \sum_{j=1}^n P_j (l_j + h_j \cot \alpha) + 12SL_0K_z}{18cf} \\
 &= \frac{139177 \text{ KNm} + 14400 \text{ KNm}}{9 \text{ m}} \\
 &= 17064 \text{ KN}
 \end{aligned}$$

4.2 Engineering verification

According to Shangwan Colliery field observations, the first weighting of 12,401 seam occurred after 40 m, its maximum weighting strength reached 507 bar (50.7 MPa). Broken key strata and discontinuous surface cracks were formed after 85 m; the first periodic weighting and partial roof fall occurred after advancing about 100 m. Hydraulic fracturing technology (Fig. 11) and a micro-seismic monitoring system (Fig. 12) were used in the 12,401 mining face. Hydraulic fracturing is of paramount importance to enhance fracturing effects in colliery hard roof control; it is a widespread process that involves blasting water and chemicals underground at high pressure to shatter the shale rock by inclined drilling [34, 35]. Micro-seismic monitoring systems have developed to a high degree in recent years as a new reference to guide safe mining: precise location of micro-seismic incidents and their intensity is realized by acoustic event monitoring, seismology, and computational geophysics [36, 37]. Micro-seismic monitoring system could be used to record micro-seismic events in both time and frequency domains to predict roof

Fig. 7 Model stress equilibrium distributions

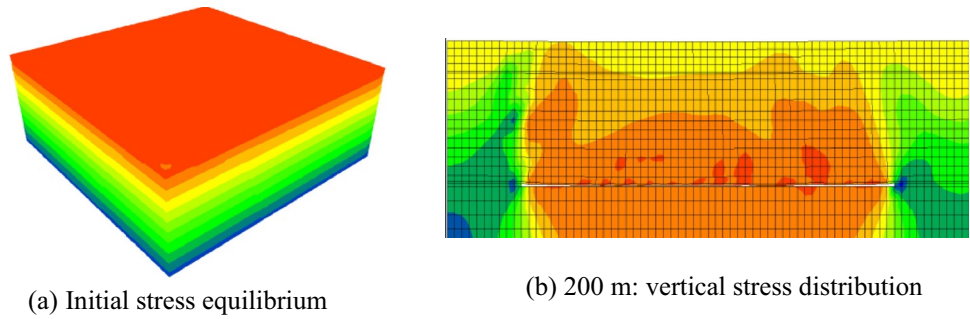


Fig. 8 Horizontal and vertical displacements at an 8.8-m mining height

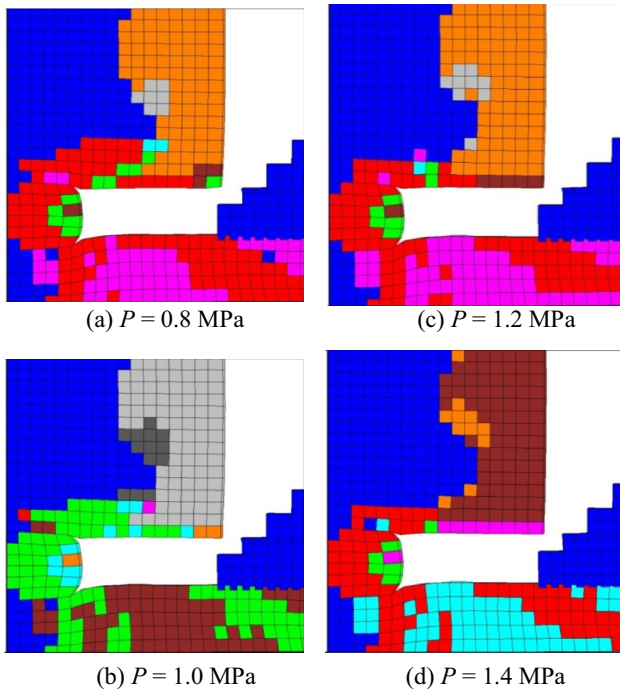
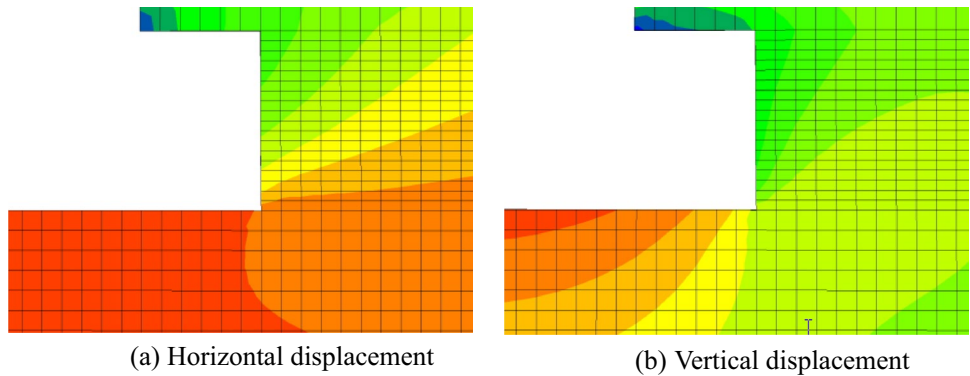


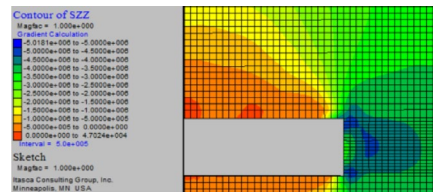
Fig. 9 Support pressure at coal failure

movement. After implementing these two measures, the 12,401 had been quickly advanced by some 4000 m and safely mined to produce 13 Mt of coal (Fig. 13), (a) shows the situation before taking measures, (b) the situation thereafter.

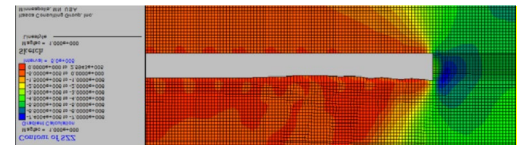
5 Conclusion

1. Support working resistances of the 12,401 mining face in small and large periodic weightings were 10,442 and 17,064 kN, which represented a loading-increase coefficient of up to 1.64. Mining cracks reached the land surface and were visible to the naked eye. The arc-shaped separation space was uneven, so the main and inferior key strata were broken and collapsed by the longwall caving method.
2. A 1.2-MPa support pressure represented the critical threshold at which engineers can effectively reduce horizontal displacement and inhibit rib spalling. Hydraulic fracturing technology and a micro-seismic monitoring system were used in the 12,401 mining face, which had been quickly advanced by 4000 m and safely mined of 13 Mt of coal.
3. The dynamic evolution of roof weighting and support, the disaster mechanism of geological structure

Fig. 10 Contours of szz at 30 m when $P = 1.2$ MPa



(a) Contours of szz at 30 m



(b) Contours of szz at 130 m

Table 3 Support pressure and maximum horizontal displacement

Support pressure/MPa	0.8	1.0	1.2	1.4
Maximum horizontal displacement/mm	482	478	458	470

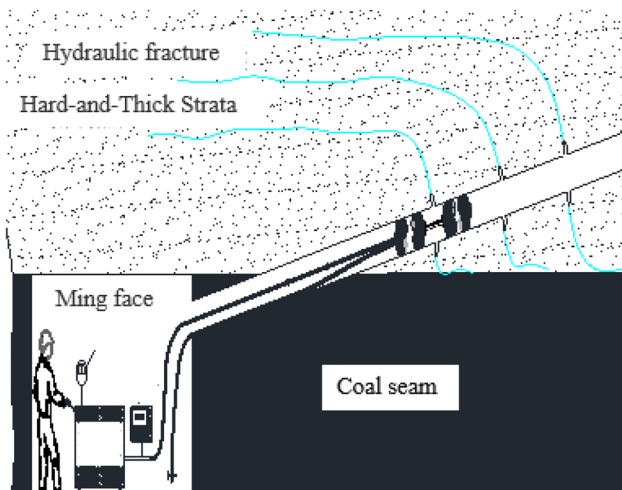


Fig. 11 Hydraulic fracturing technology



(a) Before taking measures



(b) After taking measures

Fig. 13 12,401 seam working conditions before and after taking measures

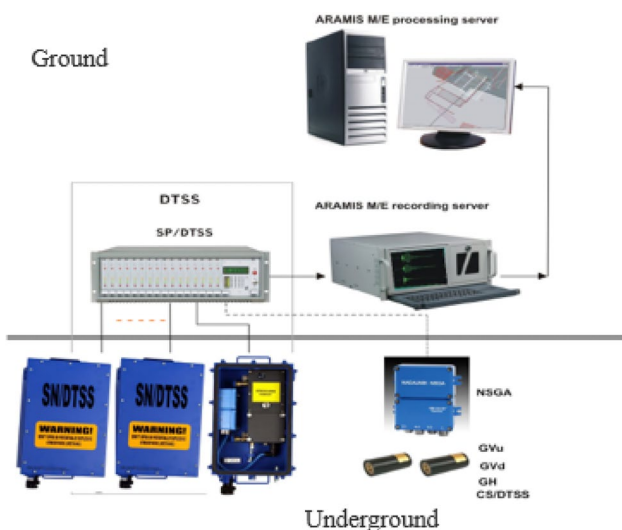


Fig. 12 Micro-seismic monitoring system

will be studied by separated layer water and tectonic stress for future research direction, which will provide new support for early warning of roof water disasters when mining coal at complex conditions.

Acknowledgements This study is supported by the Inner Mongolia Autonomous Region Natural Science Foundation (2019MS05042, 2019MS05053).

Author contributions All the authors contributed extensively to the work. MS derived the formulas and wrote the paper. ZY and XZ undertook the numerical simulation. CG and XZ conducted the field work. LQ drew the related figures and tables.

Data availability The data used to support the study are all included in the article.

Declarations

Conflict of interest The authors declare no conflicts of interest.

Open Access This article is licensed under a Creative Commons Attribution 4.0 International License, which permits use, sharing, adaptation, distribution and reproduction in any medium or format, as long as you give appropriate credit to the original author(s) and the source, provide a link to the Creative Commons licence, and indicate if changes were made. The images or other third party material in this article are included in the article's Creative Commons licence, unless indicated otherwise in a credit line to the material. If material is not included in the article's Creative Commons licence and your intended use is not permitted by statutory regulation or exceeds the permitted use, you will need to obtain permission directly from the copyright holder. To view a copy of this licence, visit <http://creativecommons.org/licenses/by/4.0/>.

References

1. Tu SH, Yuan Y (2012) Theory and practice of fully mechanized mining with large mining height in thick coal seam. China University of mining and Technology Press, Xuzhou
2. Huang QX, Zhou JL (2016) Roof weighting behavior and roof weighting of large mining height longwall face in shallow coal seam. *J China Coal Soc* 41(S1):279–286
3. Yang DF (2021) Analysis of fracture mechanics theory of the first fracture mechanism of main roof and support resistance with large mining height in a shallow coal seam. *Sustainability* 13:1678. <https://doi.org/10.3390/su13041678>
4. Huang QX, Zhou JL, Cao J (2020) Key stratum structure and support working resistance of longwall face with large mining height in the shallow coal seams, China. *Adv Civ Eng*. <https://doi.org/10.1155/2020/8834403>
5. He YP, Huang QX, Wang BQ, Miao YP et al (2019) Field-measurement study on roof breaking angle of working face with large mining height in shallow coal seam. *J Min Saf Eng* 36(4):746–752
6. Huang QX, Xu J, Du JW (2019) Determination of support setting load of large-mining-height longwall face in shallow coal seam. *J Min Saf Eng* 36(3):491–496
7. Yin XW (2019) Cutting block structure model of overburden with shallow buried coal seam and ultra-large mining height working face. *J China Coal Soc* 44(07):1961–1969
8. Wen ZJ, Xing ER, Shi SS et al (2019) Overlying strata structural modeling and support applicability analysis for large mining-height stopes. *J Loss Prev Process Ind* 57:94–100
9. Liu C, Liu ZH, Zhang JW et al (2018) Effect of mining face length on the evolution of spatial structure of overlying strata and the law of underground pressure in large mining height face. *Rock Soil Mech* 39(02):691–698
10. Wang GF, Pang YH (2018) Full-mechanized coal mining and caving mining method evaluation and key technology for thick coal seam. *J China Coal Soc* 43(01):33–42
11. Wang HW, Wu YP, Xie PS et al (2018) Coal rib stability effect of mining-thickness with large mining height of working face in steeply inclined seams. *J Min Saf Eng* 35(01):64–70
12. Xu YJ, Wang GF, Zhang JH et al (2018) Theory and application of supporting stress fields of hydraulic powered support groups in fully mechanized mining face with large mining height based on elastic supporting beam model. *Chin J Rock Mech Eng* 37(05):1226–1236
13. Fan ZZ, Qi QX, Wang JC (2018) Method and application of mining intensity evaluation model in large mining height working face. *J Min Saf Eng* 35(02):347–351
14. Wang GF, Pang YH, Li MZ et al (2017) Hydraulic support and coal wall coupling relationship in ultra large height mining face. *J China Coal Soc* 42(2):518–526
15. Zhao YX, Jiao ZH, Liu HB et al (2017) Simulation of ground pressure distribution at large mining height face based on GIS techniques. *J China Univ Min Technol* 46(01):33–40
16. Kong DZ, Yang SL, Gao L et al (2017) Determination of support capacity based on coal face stability control. *J China Coal Soc* 42(03):590–596
17. Huang QX, Tang PF (2017) roof weighting analysis on large mining height longwall face in shallow coal seam. *J Min Saf Eng* 34(02):282–286
18. Zhang HL, Tu M, Cheng H et al (2017) Roof leakage mechanism and control technology study of fully mechanized large mining height mining face of thin bedrock seams. *Rock Soil Mech* 38(06):1697–1704
19. Huang QX, Zhou JL (2016) Roof weighting behavior and roof weighting of large mining height longwall face in shallow coal seam. *J China Coal Soc* 41(S2):279–286
20. Wang G, Luo HZ, Wang JR et al (2016) Broken laws of key strata on strata behaviors in large height fully-mechanized face of nearly shallow coal seam. *J China Univ Min Technol* 45(03):469–474
21. Yang SL, Wang ZH, Kong DZ et al (2016) Overlying strata failure process and support resistance determination in large mining height face. *J Min Saf Eng* 33(02):199–207
22. Guo WB, Yu XY, Zhao BC et al (2016) Experimental research on catastrophic mechanism of overburden strata with high excavation height in high tectonic stress zone. *J Min Saf Eng* 33(06):1058–1064
23. Wang ZH, Yang JH, Meng H (2015) Mechanism and controlling technology of rib spalling in mining face with large cutting height passing through fault. *J China Coal Soc* 40(01):42–49
24. Xie PS, Wu YP, Wang HW et al (2015) Interaction characteristics between strata movement and support system around large mining height fully-mechanized face in steeply inclined seam. *J Min Saf Eng* 32(01):14–19
25. Yang SL, Kong DZ (2015) Flexible reinforcement mechanism and its application in the control of spalling at large mining height coal face. *J China Coal Soc* 40(06):1361–1367
26. Chang JC, Xie GX, Zhang XH (2015) Analysis of rib spalling mechanism of fully-mechanized top-coal caving face with great mining height in extra-thick coal seam. *Rock Soil Mech* 36(03):803–808
27. Yin SF, He FL, Cheng GY (2015) Study of criteria and safety evaluation of rib spalling in fully mechanized top-coal caving face with large mining height. *J China Univ Min Technol* 44(05):800–807
28. RayChowdhury A, Pramanik A, Roy GC (2021) New approach for localization and smart data transmission Inside underground mine environment. *SN Appl Sci* 3:604. <https://doi.org/10.1007/s42452-021-04589-2>
29. Qian MG, Shi PW, Xu JL (2010) Ground pressure and strata control. China University of Mining and Technology Press, Xuzhou
30. Liu ZY (2014) Strata behavior of ultra-close-multiple coal seams under gob in fully mechanized caving face and its control. China University of mining and Technology, Beijing
31. Feng Q, Liu WW, Fu SG et al (2017) Analytical solution for deformation and internal force of hard roof in stope based on elastic foundation beam. *J Min Saf Eng* 34(02):342–347
32. Wang H, Gao YT, Jin AB et al (2014) Determination of stiffness parameters of jointed rock masses with 3DEC simulations. *Chin J Rock Mech Eng* 33(S1):2894–2900
33. Chen YM, Xu DP (2013) FLAC/FLAC3D foundation and engineering example, 2nd edn. China Water Resources and Hydropower Publishing House, Beijing

34. Klishin V, Nikitenko S, Opruk G (2018) Longwall top coal caving (LTCC) mining technologies with roof softening by hydraulic fracturing method. *IOP Conf Ser-Mater Sci Eng*. <https://doi.org/10.1088/1757-899X/354/1/012015>
35. Sun Y, Fu Y, Wang T (2021) Field application of directional hydraulic fracturing technology for controlling thick hard roof: a case study. *Arab J Geosci* 14:438
36. Ding YL, Dou LM, Chen JJ, Kong Y, Su ZG, Li ZL (2016) Signal characteristics of coal and rock dynamics with micro-seismic monitoring technique. *Int J Min Sci Technol* 26(4):683–690
37. Sun YJ, Zuo JP, Li YB, Liu CH, Li YH, Shi Y (2017) Micro-seismic monitoring on fractured zone and water inrush mechanism analysis of deep mining above aquifer in Xingdong coalmine. *Rock Soil Mech* 38(8):2335–2342

Publisher's Note Springer Nature remains neutral with regard to jurisdictional claims in published maps and institutional affiliations.